Appl Phys B (2009) 96: 601–611
DOI 10.1007/s00340-009-3521-0

Applied Physics B
Lasers and Optics

Laser-induced incandescence: excitation and detection conditions, material transformations and calibration

R.L. Vander Wal

Received: 12 January 2009 / Revised version: 12 March 2009 / Published online: 5 May 2009

Abstract Successful implementation of laser-induced incandescence (LII) relies upon judicious choice of excitation and detection conditions. Excitation conditions encompass choice of excitation wavelength and laser fluence. Detection conditions include choice of detection wavelength, spectral band pass about the central wavelength, detection delay and duration relative to the excitation laser pulse usually corresponding to the peak of the signal intensity. Examples of applying these parameters to LII are illustrated by way of examples: soot/polycyclic aromatic hydrocarbon and metal aerosol systems. Tradeoffs must be recognized. Laser-induced chemical and structural changes of the aerosol must be considered, particularly in light of heterogeneous aerosols. Diagnostics of such changes are outlined as they will affect interpretation of the LII signal. Finally, calibration (for LII) must be chosen to be appropriate for aerosols from practical sources as they may be mixed organic and inorganic composition.

PACS 78.47.Cd · 85.60.Gz · 42.62.Fi · 44.40.+a · 65.80.+n

A research paper in response to the call for papers from the Third International Discussion Meeting and Workshop on Laser-Induced Incandescence July 30th–August 1st, Ottawa, Canada (2008).

R.L. Vander Wal (✉)
Department of Energy and Mineral Engineering, The Energy Institute & The Penn State Institutes of Energy and the Environment, Penn State University, 203 Hosler Building, University Park, PA 16802, USA
e-mail: ruv12@psu.edu
Fax: +1-814-8635709

1 Introduction

Since its inception, laser-induced incandescence (LII) has been applied to qualitative spatial and temporal distribution of soot and quantitative soot volume fraction and primary particle size measurements [1]. Models are frequently used to analyze LII data, particularly time-resolved signals recorded for primary particle sizing [2–8]. In essence all models solve the basic energy conversation equation with input from laser absorption and cooling via the time-varying, relative contributions of evaporation, radiation and conduction to the surroundings [9–15]. Within this framework the excitation parameters may be viewed as direct inputs into the energy balance whereas the detection parameters are to be chosen guided by the spectral and temporal evolution of the signal as predicted by the model. They are not explicit outputs per se. Depending upon the model's sophistication, experimental signal collection can be guided and optimized for sensitivity or insensitivity to primary particle size, for example. Current efforts have identified specific soot physical constants such as the refractive-index function and thermal and mass accommodation coefficients as responsible for large divergences between different models, particularly at high laser fluence [16].

Yet, practical considerations apart from the soot heating and cooling processes as treated by models are particularly important. Primarily these are laser-induced interferences in the form of fluorescence [17], phosphorescence or even incandescence from co-present, non-soot particles [18]. Such photophysical processes are not formally included in LII models within the energy balance formalism. These parameters often set the real constraints in selecting excitation and detection parameters. Secondly, with the exception of a recent model that includes phase changes and oxidation, mod-

els do not account for time (i.e. temperature) varying properties during the course of heating and cooling. Moreover, no physical or chemical changes in the particle are considered to occur. Yet, work in this laboratory has shown substantial laser-induced transformations in carbon aerosols, both by post-LII microscopy analysis on extracted samples and by in situ diagnostics [19, 20]. In some cases such morphological and structural changes can be minimized, while for other systems they are unavoidable. Consideration of such changes may guide selection of excitation parameters. Finally, the initial aerosol physical and chemical composition may mandate selection of excitation and detection conditions.

Soot is formed in environments containing polycyclic aromatic hydrocarbons (PAHs) and often is composed of such species, more generally referred to as organic carbon [21]. Other aerosols may not be carbon based. Well-known examples include fumed TiO_2, SiO_2 and metals or metal–dielectric combinations [22]. Additionally, combustion emissions can produce aerosols of metal oxides and metals. Yet other aerosols may consist of a mixture of carbon and metal species. A well-known example is flame synthesis of carbon nanotubes [23–27]. In each system it is desirable to measure concentration and/or to have an online process diagnostic. LII has this capability. In the context of excitation and detection strategies, this statement needs to be examined. General recommendations may not hold for non-traditional aerosols and specific conditions need to be evaluated on a case-by-case basis.

2 LII Excitation and detection issues

Broadly, implementation of LII requires attention to four experimental variables as grouped by excitation and detection conditions as illustrated in Fig. 1. Excitation encompasses laser fluence and wavelength while detection pertains to the spectral and temporal collection intervals for the LII signal.

These four parameters are not arbitrary, nor strictly experimental parameters. For example, excitation wavelength and fluence are also key input parameters for LII models. Model outputs are the spectral and temporal profiles of the LII signal. Such knowledge is critical to assessing possible biases imposed by varying particle sizes, effects of vaporization, conductive rates of cooling and lower heating within the beam wings. While excitation and detection conditions have been discussed previously [28, 29], they are hereafter considered in the context of aerosols of mixed composition, non-carbonaceous aerosols and laser-induced transformations in both. These two categories are discussed next followed by real examples in Sect. 3 illustrating the general principles involved.

Laser excitation wavelength, see Fig. 1a, is dictated by the rather finite values of available laser wavelengths (while avoiding wavelengths that are on resonance with atomic or molecular constituents). To avoid exciting spectral interferences such as fluorescence or phosphorescence, visible or even near-infrared wavelengths are preferable. Fortunately the absorption of soot and the elemental components of carbonaceous aerosols are sufficiently broad that excitation wavelengths from UV–Vis to the infrared may be effectively used. However, oxides of light elements, e.g. SiO_2, TiO_2, or non-metals, e.g. sulfate, may not absorb at such wavelengths; generally infrared or far-infrared frequencies are required.

Laser excitation fluence, see Fig. 1b, is determined by the absorption coefficient of the material. Lower absorption coefficients require higher fluence to produce incandescence in the visible region. For nanosecond pulse lengths and greater,

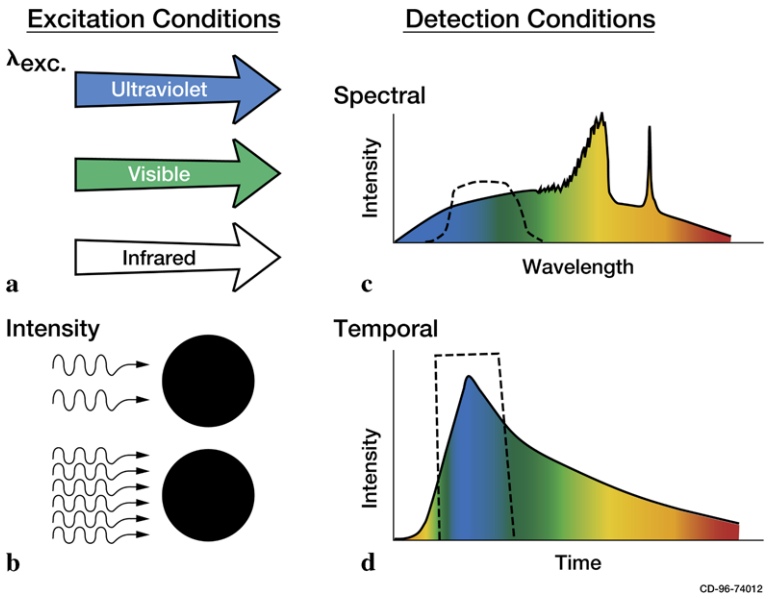

Fig. 1 Schematic illustrating excitation and detection conditions for LII. Excitation refers to laser wavelength and fluence. Detection refers to the spectral and temporal region over which the LII signal is collected

fluence is the operative parameter as the electronic excitation will be converted to heat on time scales short relative to the particle heating. For picosecond and especially femtosecond laser pulses, particle electronic excitation has not been converted to thermal energy and further input of high-intensity laser light will continue to excite free electrons to the vacuum level, effectively stripping them from the particle [30]. The resulting charge imbalance in the particle induces particle exfoliation of the surface layers and even Coulombic explosion if absorption proceeds volumetrically. This is a largely unexplored regime of LII and it would appear difficult to control.

Detection conditions encompass spectrally where and temporally when to collect the signal. Figures 1c and d illustrate the spectral and temporal characteristics of the LII signal. Often the signal is detected in the near ultraviolet because the quantum efficiency of photocathode materials peaks in this region and combustion luminosity is far lower in intensity than at longer wavelengths.

Attempts to fit such spectra to black-body curves however have met with limited success. This likely reflects the variation of particle temperatures due to both the variation in laser intensity across the laser beam profile [12] and the distribution of soot primary particle sizes resulting in varied cooling rates [16]. Regardless of the fit, the utility of such information is that laser-induced spectral interferences can readily be identified. These interferences arise from electronically excited small molecules or radicals produced by the high-intensity laser light which can fluoresce in the wavelength interval in which the LII signal is collected. Such signals are experimental artifacts, not necessarily representative of the soot concentration and should be avoided if an incandescence signal is desired [31].

Illustrated in Fig. 1d, the emission from the laser-heated soot rapidly rises, reaching a peak and subsequently decays after the excitation laser pulse. The decay reflects the cooling of the soot via radiative and conductive heat transfer processes [9–15]. Empirical studies have shown that the best measure of soot concentration is obtained by detecting the LII signal during and shortly after the excitation laser pulse (within a few tens of nanoseconds) [29]. During this time period, different cooling rates associated with different primary particle sizes have the least effect on the particle temperature and consequently upon the LII signal [2–8]. Numerical evaluation of such dependences is challenging. Uncertainty regarding the accommodation coefficient in heat transfer from the laser-heated aerosol still exists [10–13].

Of course, prompt temporal detection of the signal is only accurate provided that spectral interferences can be avoided by detecting other wavelengths to serve as a measure of the incandescence intensity. If not, delayed detection of the LII signal can be used since fluorescence interferences are generally short-lived relative to the LII signal [28, 31]. It is best to avoid such interferences by the use of long-wavelength excitation [6, 23]. At longer excitation wavelengths, fewer electronic resonances exist to produce electronically excited molecules and radicals that may fluoresce [17, 21]. Following are examples illustrating application of these considerations.

3 Selected illustration of excitation and detection conditions

3.1 Soot/PAH—illustrating excitation laser wavelength and detection time interval

Soot forms through a complex process of fuel pyrolysis processes and molecular growth. In combustion systems using practical fuels, molecular growth through PAHs can occur directly given the nascent high aromatic content of the fuel. Yet other systems including engines and gas turbines feature high mixing rates and can induce pyrolysis via oxygen-mediated reactions.

With increasing molecular size the number of electronic states increases while the energy gap between the highest occupied molecular orbital (HOMO) and lowest unoccupied molecular orbital (LUMO) decreases [32]. As the electronic state density increases so too does the rate of non-radiative relaxation processes. Molecular fluorescence decreases at the expense of molecular heating via intramolecular dissipation of absorbed energy. Yet, there is a definite boundary between molecules and solid-state matter. At some point (and the definition depends upon the measurement method and purpose), the particle structure attains bulk properties. For carbon-based soot formation within flames this transformation has been discussed in terms of carbonization [33]. The net result is that incandescence occurs instead of fluorescence [34].

Within the environment in which soot forms, PAHs are prevalent both as gaseous compounds and as nucleated aerosols known as soot precursor particles [21, 33, 34]. Use of long-wavelength irradiation such as 1064 nm will generally avoid excitation of PAHs while yet accessing sufficient absorption of soot to cause incandescence. However, the use of 532 nm has been prevalent within the literature given its ease of use and readily available sources. Light at 532 nm can excite fluorescence from large PAHs. The potential for fluorescence interference is even worse if using 355-nm or 266-nm laser light [17].

Fluorescence is the most common spectral interference. As stated, using 1064-nm excitation will avoid PAH fluorescence. Alternatively delayed detection can also avoid fluorescence contamination of the LII signal. Fluorescence occurs within the nanosecond time scale at atmospheric pressure [33, 34]. Though molecular and atomic radiative

lifetimes can be large, collisional quenching induces non-radiative decay channels leading to a loss of radiation. In contrast, the incandescence radiation is dominated initially by radiative cooling (for temperatures >3000 K) and collisional cooling for lower temperatures. Thus, with a delayed gate relative to the excitation laser pulse fluorescence can be missed while incandescence is yet captured [29].

3.2 Metals and oxides—illustrating excitation laser fluence and detection wavelength

Metal aerosols hold promise for a number of applied nanotechnology applications as well as being a direct environmental pollutant produced by combustion [35]. Metals have a very high energy level density and absorb over a broad spectral region. Yet, their vaporization temperatures are relatively low and, with the exception of a few elements such as W, Nb, Ta and their carbides, their melting points are nowhere near that of carbon. With detection (and calibration of LII via extinction) most easily performed in the visible region of the spectrum, there is strong motivation to heat the particles sufficiently to shift their incandescence spectrum further into the visible region for detection purposes. However, attempts to further increase particle temperature by superheating using high laser fluence will only result in particle vaporization.

In general, this has been avoided (for LII applied to soot) given observations of spectral interferences such as atomic and molecular emission contributing to and contaminating the incandescence. In the case of limited incandescence potential, particularly for relatively low melting point metals such as Fe, this may be a practical alternative. In fact, our own studies of LII applied to W and Fe nanoparticles revealed no such interferences [36]. However, it should be noted that this vaporization regime is largely uncharted territory for which there is a dearth of experimental or theoretical backing. Spectrally resolved emission curves indeed illustrated pseudo black body emission, now understood as arising from the laser-induced microplasmas of each particle in the beam path. There is also the potential limitation that the high fluence will cause excessive heating of the vaporized plasma by inverse Bremsstrahlung absorption. This was not observed to be the case in our studies [36].

A key advantage of judicious wavelength selection is that laser fluence can then be selected based upon either fluence-dependence measurements or by maximizing the LII intensity and temporal evolution of the incandescence signal. Maximizing the intensity coincides with maximizing the incandescence, while maximizing the temporal evolution ensures avoidance of vaporization (resulting in material loss and faster cooling of the residual, 'solid' carbon giving rise to the incandescence).

When collecting LII from metals with low melting and vaporization temperatures, the possibility exists that electronically excited species are created in the excitation process. If operating in a complete evaporation regime, this is even more a distinct possibility. Atomic and small molecule emissions can be identified by their narrow spectral features compared to the broad spectral emission of incandescence [17, 18]. However, low intensities of such emission can be masked by the incandescence signal. Therein, the only recourse to look for such potential interferences is full spectral resolution of the signal with black-body fitting to verify incandescence and its continuance with time. In turn, this requires spectral and temporal detection hardware in the form a spectrograph and gated ICCD, respectively.

In summary, the choice of spectral region for detection is determined on the basis of detector sensitivity, particle concentration and what regime in which to operate, i.e. true incandescence arising from condensed matter or from the plasma produced by laser vaporization. Notably, this latter route would presumably provide a proportional signal, even though it is not true 'incandescence' and can be convolved with spectral interferences.

4 Laser-induced aerosol transformations

The action of pulsed laser light can induce any number of possible changes in the absorbing aerosol as illustrated in Fig. 2. For example, rapid volatilization of molecular fragments or substituents can initiate particle breakup, i.e.

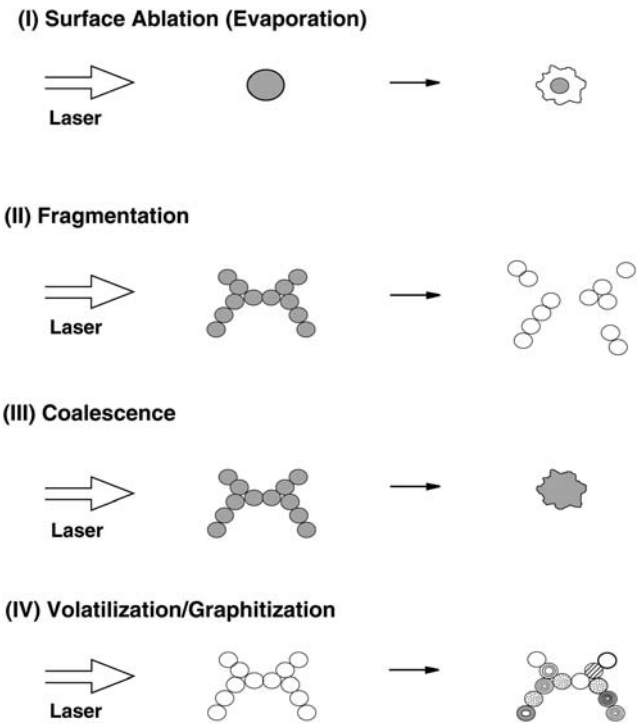

Fig. 2 Illustration of the possible morphological and structural changes that may occur in an aerosol subjected to high-intensity laser radiation such as in LII

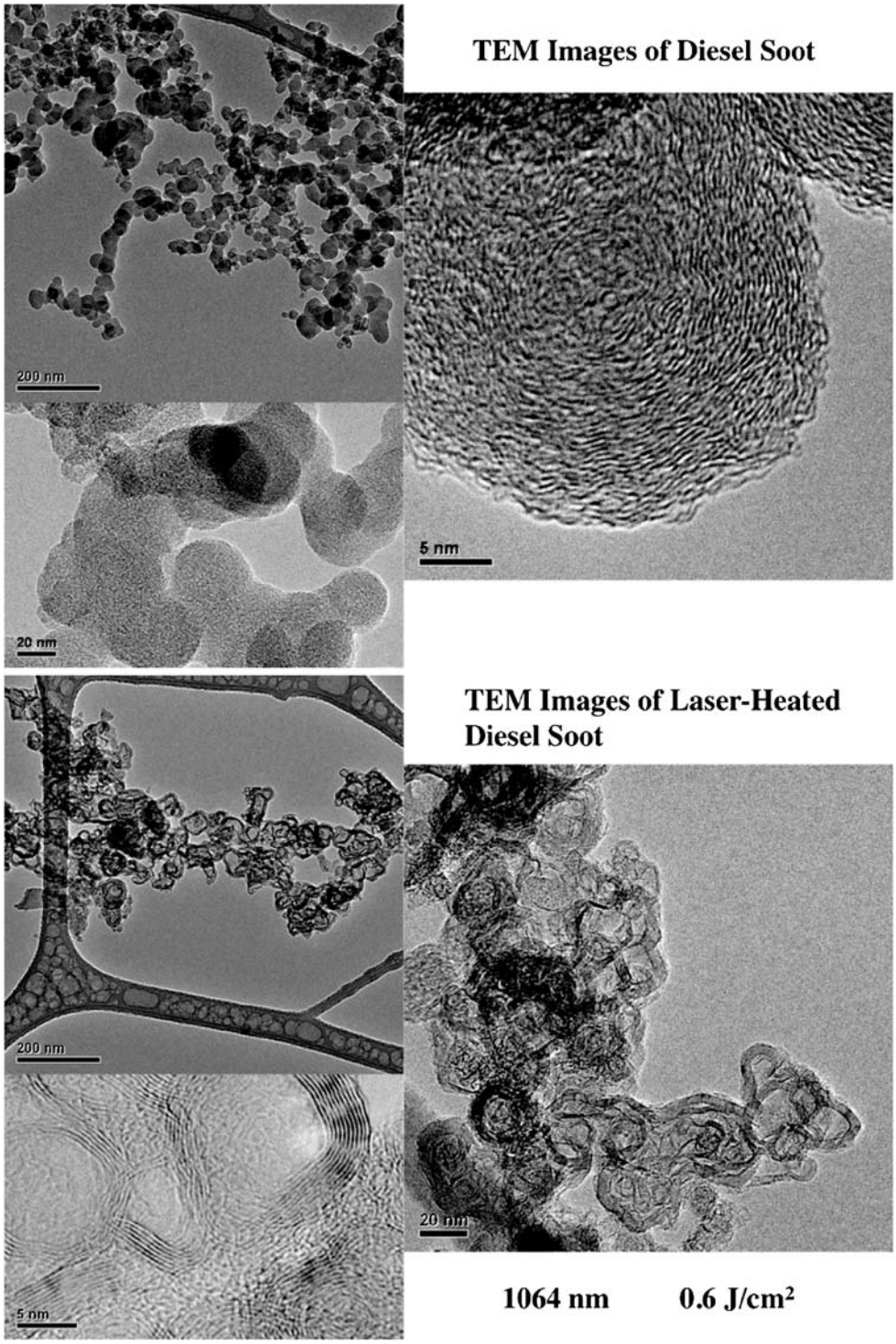

Fig. 3 TEM images of soot prior to LII (*top panel group*) and after LII (*bottom panel*). Each panel shows three magnifications. The lowest magnification shows that aggregate morphology is relatively unchanged at this laser fluence. The intermediate magnification shows that the carbon within primary particles undergoes substantial restructuring. The high magnification reveals the changes in the individual carbon lamellae

fragmentation. Alternatively, if the particle melting point is reached and there is sufficient difference between the melting and vaporization temperatures, coalescence can occur. If the vaporization temperature is relatively low or sufficiently high laser fluence is utilized, particle vaporization will occur. Finally, as has been observed in other carbon materials, annealing can occur.

Figure 3 shows a transmission electron microscopy (TEM) image of a soot particle before and after being subjected to pulsed laser light at 1064 nm from a Nd:YAG laser. (The first TEM image shows a representative nascent particle.) That annealing of the carbon occurs upon high-temperature heating is a well-known occurrence [37], particularly in the area of soot oxidation where a graphitic

soot, featuring fewer edge site carbon atoms relative to basal plane positions, has markedly lower reactivity towards oxidation [38]. The surprising feature here is the time scale of the transformation [29]. Necessarily the material transformation has occurred while the carbon is at elevated temperatures, namely above 2000°C, a temperature commonly considered as a graphitization threshold based on traditional heating studies.

During the pulsed laser heating C–C and C–H bonds will break within picosecond time scales. Therein, lamella mobility is enabled and the soot nanostructure can relax into a more thermodynamically stable graphitic lattice structure. Kinetically limited, this transformation occurs while the particle is at elevated temperature, being most facile when the particle temperature is above 3000°C, corresponding to the same time frame during which the LII signal is collected.

While fascinating from a material science perspective, such a dynamic lattice transformation on the nanosecond time scale raises many questions as to the interpretation of the LII signal [18, 20]. With carbon morphology and density changing, the optical properties are also likely altered. Given that LII relies upon other techniques for absolute calibration suggests that such considerations are not of great import. Even so, LII diagnostics of these changes in the form of pump–probe experiments show that these nanostructural changes do indeed impact the LII signal [18, 20] because they occur within the same time frame as the signal collection.

Using two laser pulses of variable fluence, our prior studies showed that the LII signal generated by the second pulse was dependent upon the fluence of the first laser pulse [18, 20]. While one would expect this to be the case for fluences (of pulse 1) above the vaporization threshold, this also held for fluences below the vaporization onset [19]. Such changes in the LII signal produced by a second pulse of identical energy confirm that the morphological and structural changes occurring in the soot do indeed affect the LII signal [18, 20]. More specifically, changes in LII parameters such as fluence, wavelength and spectral or temporal detection may cause the signal to scale in a non-predictable manner if particle physical and chemical changes occur within the heated particle. While calibration perhaps should be performed for any such change in LII parameters, it is often not practical. Moreover, other subtleties apply. The laser beam profile is non-uniform and at best is approximated by a Gaussian that will produce a range of soot particle temperatures across its profile [12]. Different portions of the beam wings are collected depending upon the optical collection volume [12]. Additionally, the laser intensity may be attenuated along the measurement path due by soot absorption [28, 29].

5 Mixed aerosols

Mixed material systems are inevitable in applied situations. Fuels for power generation, coal or heavy fuel oil contain significant contaminants. From sulfur-rich fuels, combustion particulates can contain tens of percent elemental sulfur content. Carbonaceous aerosols can contain a high fraction of organic and elemental carbon. With increased emission regulations and use of diesel engine particulate filters (DPFs) to achieve compliance, non-carbon ash from lubricants now comprises a significant fraction of mass emission indices from heavy-duty diesel engines. Interestingly, biofuels can lead to soot with varying degrees of residual oxygen content and a substantial fraction of sp^3 hybridized carbon compared to nominal sp^2 hybridization. The former is associated with fully saturated hydrocarbons or alkyl chains while the latter is characteristic of graphite and heavy aromatics. This heterogeneity imposes the need for the following considerations [18]:

1. relative mass fractions of the different components
2. melting temperature and vaporization temperature differences and
3. reactivity of each material towards the other.

The first two considerations pertain as to what material dominates the LII signal and the fraction of LII available from each material. Clearly, the melting temperature dictates the upper bound for particle heating unless ‘mixed-phase’ LII is pursued where one component is completely vaporized while the other remains in a solid state to incandesce. This is an unlikely scenario for multiple-component aerosols as the vaporization of one component will likely induce significant fragmentation of the particle matrix.

The third criterion is perhaps the most interesting but also potentially problematic. An example drawn from material synthesis is measuring carbon nanotubes in the aerosol phase. One motivation would be in a manufacturing setting for production monitoring or to gauge worker exposure. Carbon nanotubes, multi-walled (MWNTs) or single-walled (SWNTs), contain catalyst metal. For MWNTs this can range typically from 0.5 to 3 wt.% while for SWNTs values can range from 10 to 40 wt.% depending upon the synthesis process. Catalysts for SWNTs are generally Fe with minor fractions of other elements such as sulfur, Ni or other transition metals, while MWNT catalysts are more varied [40–42]. Clearly, for MWNTs the low metal content and low (compared to carbon) melting and vaporization temperatures suggest that the metal incandescence can be neglected if only a carbon mass signature is desired, while both materials will be observed for SWNTs. Here, vaporization could impose significant material changes. A second consideration is that the different morphology of these nanocarbons introduces ther-

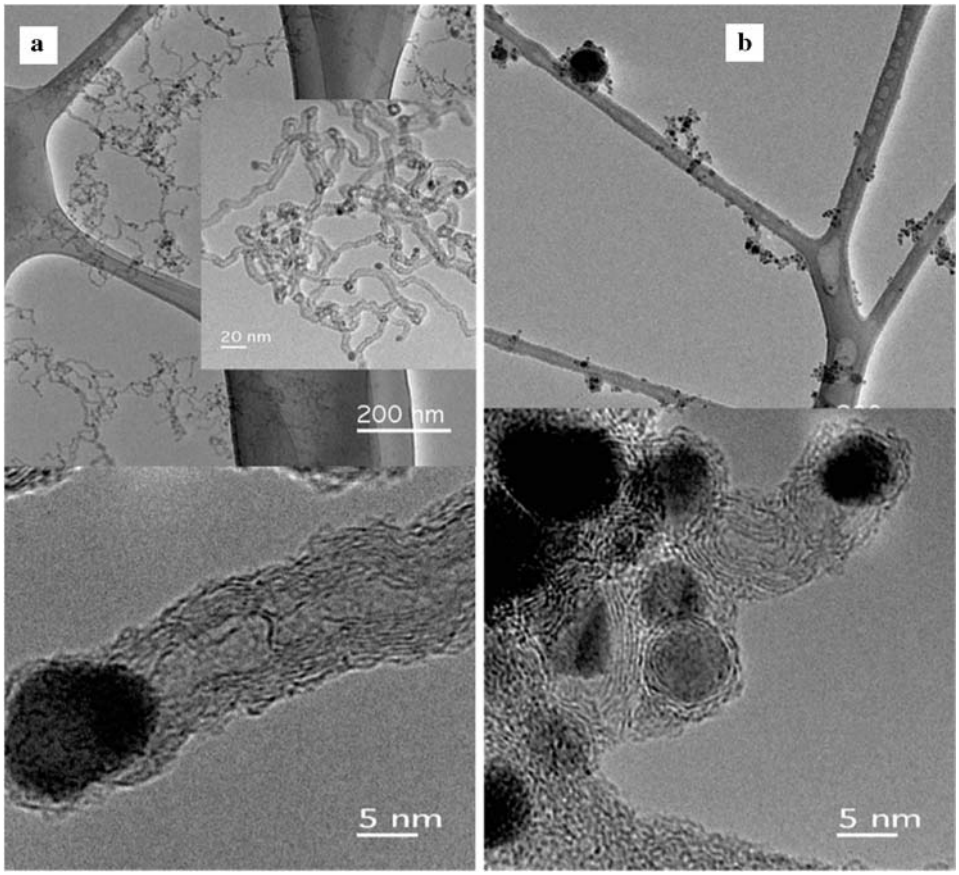

Fig. 4 TEM images of nascent MWNTs (column **a**) and after LII (column **b**). The dark particles are the catalyst metal. The MWNTs are not purified but shown as prepared. The action of LII appears to not induce graphitization but rather coalescence of metal nanoparticles and reformation of carbon around them in the form of shells. Such shells likely arise through carbon dissolution from the catalyst upon cooling below the metal–carbon eutectic

mal instability, in particular for SWNTs. Past ∼1600°C, the precise temperature depending upon the SWNT diameter, SWNTs deconstruct into random carbon or occur as so-called 'ropes', i.e. bundled into MWNTs. A third possibility is the renewed interaction between carbon and metal. CNTs grow by metal-catalyzed hydrocarbon decomposition and carbon precipitation [40]. Although temperature can vary considerably, a typical synthesis temperature range for MWNTs is 500–900°C for MWNTs and 800–1000°C for SWNTs. At temperatures below these values the interaction between metal and carbon ceases but can resume upon laser heating. LII temperatures far exceed those for synthesis however and most likely a single-phase system evolves. The fast cooling characteristics of LII would quench the metal–carbon mixture from this intermediate state.

We addresed these issues by applying LII to SWNTs and MWNTs as synthesized directly in the aerosol phase through our flame-based synthesis method [23–27]. As an example of the action of pulsed laser light on these heterogeneous materials, Fig. 4 shows a nascent and annealed (post-LII) MWNT [43]. In summary, LII morphological changes will be more prevalent in heterogeneous aerosols [43].

6 Diagnosing laser-induced chemical and physical changes in aerosols

Given such possible interferences in interpreting the LII signal, the operative question is how to tell if they are occurring, particularly in non-carbon systems? Four options may be exercised, with varying degrees of success. First, fluence-dependence curves have been universally applied to identifying an appropriate value of excitation fluence. Measuring the signal as a function of fluence can detect vaporization by the decrease in signal but only after the point at which significant vaporization is occurring [16, 20, 28].

The spectral and temporal evolution of the LII signal is a second more sensitive measure of vaporization or other laser-induced transformations such as fragmentation or annealing [18, 20]. With smaller particles and/or mass loss, the LII signal will decay faster [2–11, 16, 44]. Spectral changes can detect vaporization or the release of atoms or small molecules by their narrow distinct spectral emission if this intensity overcomes the incandescence. In our experience the plasma resulting from vaporization/ablation of aerosols (fortunately) is not an efficient method for producing electronically excited fragments when using 1064-nm excitation

light [17, 21, 31, 34]. If structural changes occurred that induced a change in optical properties, this might be detectable via spectrally resolved emission [18, 20]. This has yet to be identified, however. Temporally resolved spectral emission can be a sensitive measure of structural changes that affect the cooling rate and hence time evolution of the signal [18, 36]. Nevertheless, the most rigorous means of identifying any type of material alteration is a repeated measurement. As applied to LII this would take the form of a pump–probe experiment, as we have demonstrated [18, 20].

The fourth method involves direct TEM visualization of the laser-heated material. Extractive sampling for subsequent microscopy is the most definitive method for identifying laser-induced changes [18–20, 28, 39]. Such data complements direct optical measurements by providing insights into the impact of structural changes upon the LII signal.

It is interesting that the one LII model that incorporates both oxidation and phase change predicts a distinctly longer time evolution of the signal than most other contemporary models under low fluence but shorter than most at high fluence [16]. For other conditions it is difficult to resolve differences. Currently there is yet a gap between these advanced models and experiments. Models do not include or generate particle nanostructure such as observed by high-resolution TEM (HRTEM) [16]. Alternatively, and as illustrated, experiments can be designed to spectrally assess the magnitude of the laser-induced change and temporally resolve the course of this evolution. To assess a model as capturing the relevant physical and chemical changes will require it be applied to both types of measurements. Of foremost importance will be inclusion of soot nanostructure by which nascent or laser-graphitized soot can be included in a model. Only then can the critical question as to the impact of these changes upon the LII signal be assessed.

7 Calibration

LII is a relative measurement method. Hence, it relies upon a secondary measurement to provide calibration. It is yet debated as to whether theory is sufficiently evolved as to interpret a priori the LII signal in absolute mass. Material changes only add to the assumptions and questionable success of this approach. Hence, empirical calibration is not only preferred but necessary. Some caveats on popular methods are briefly discussed next.

7.1 Extinction calibration

Extinction methods are the most general method of calibrating LII using either line-of-sight or tomographic methods [45]. The limitations on extinction methods are (a) accurately accounting for scattering contributions, and (b) uncertainty in optical constants of the aerosol, particularly if a mixed system (e.g. organic/elemental carbon, inorganic and organic, etc.). Moreover, there is the implicit assumption that the absorbing components at the extinction measurement wavelength are those that will absorb 1064-nm light and remain in condensed phase (solid or liquid) to incandesce. PAHs in particular will not yield incandescence even though five-ring and larger ones will contribute to extinction [32]. Soot precursor particles prior to carbonization will also contribute to a false calibration of LII by absorption. More generally, the implicit assumptions that the chemistry and by inference optical properties of soot remain constant are generally false. Soot from laboratory hydrocarbon flames has an H/C atom content generally between 0.1 and 0.2. Soot from practical sources such as diesel engines may have H/C ratios between 0.1 and 0.4, depending upon the load, fuel, etc. The LII action will drive off the H-atom content [19, 39]. The impact of hydrocarbons and H-atom content upon the LII signal at different controlled concentrations has not been tested.

7.2 Two-color approach—calibration

Recently, an ingenious method for LII calibration was demonstrated based on optical pyrometry in a so-called two-color approach [46–48]. In this method a calibrated W strip lamp is measured at two separate wavelengths. Their ratio, given the known lamp calibration, permits finding an optical system detection correction for emission at the two wavelengths, as a ratio. This stems from application of Planck's law and known black-body radiation from the lamp at a specified temperature. Observation of the LII signal at these same two wavelengths (intervals) along with this information permits solving for temperature and soot volume fraction. Important parameters include excitation laser beam profile, soot composition, structure and optically thin conditions.

7.3 Gravimetric sampling

The surest method of measuring emitted mass is by filter collection [49]. Prior to implementation of emission standards this approach was not a problem for heavy-duty (HD) diesel engines. However, with today's standards, these emissions produce a negligible mass fraction of carbon soot under normal engine load. After 2007 every new HD diesel truck is fitted with a diesel particulate filter (DPF) to meet the EPA tier 4 emission standards. Particle capture efficiency exceeds 98% with such after-treatment devices. However, nanoparticles emerge from such traps. These consist of nucleation-mode particles based on sulfate, ash from lubrication oil compounds and carbon remnants from the trapped and oxidizing soot particles that eventually reach a small enough size to escape the filter. The low carbon emissions from

such exhaust systems render the traditional method of exhaust measurement based on the smoke meter useless. Yet, the need remains to measure the particle mass and number concentration in the exhaust. LII is a prime candidate. Still, calibration by filter collection will be exceedingly challenging and, even if sufficient mass is collected, it will contain a very high fraction of inorganics and give a false interpretation to LII signals based on such values.

As an example Table 1 lists elements and their percentages as measured by X-ray photoelectron spectroscopy (XPS) for soot from a gas-turbine engine running Jet A fuel. The role of carbonaceous particle emission from jet engines in global warming and rainfall patterns is prompting increased study of this source [50]. LII has the potential for real-time, field measurements. Notably, the soot contains a high percentage of non-metals, especially sulfur and oxygen. The implications for such elemental variability upon the LII signal have yet to be deciphered.

To further drive home the point of heterogeneous composition, additional XPS data confirm the mixed carbon composition of this soot. Figure 5 shows an XPS scan over the nominal C1s region. Deconvolution of the C1s component yields the sp^3 and sp^2 contributions to the carbon signature peak. Sp^2 carbon is that associated with an aromatic structure and in particular the graphene segments comprising the elemental carbon component. The sp^3 hybridized carbon corresponds to the alkyl groups either as substituents to aromatic structures and/or an organic compound containing H and O atoms within the carbonaceous particulate. This fraction may be considered as the organic component of the aerosol [51].

Short of such external methods, the only recourse is to interpret the signal in light of model predictions. In this 'absolute' approach, a LII signal characteristic is equated to a model's output/prediction and remaining parameter inputs to the model are then taken as describing the experimental environment. With either a spectrally or temporally resolved signal, this approach has been applied for primary particle size. Combined, this approach can be applied to determine soot volume fraction, f_v, with optical collection and detection system corrections [46–48]. Alternatively, reference flames have been used successfully and they also offer the ability to develop a calibration curve and investigate the dependence upon soot particle parameters by varying the combustion conditions.

Table 1 Listing of heteroelements in soot collected from the jet engine of an A300 aircraft. Interestingly, soot from a Lear jet also contained the same elements while the emissions from a DC-9 contained no elements past Si, illustrating the variability and signature of heteroelements from different sources

Element	Percent concentration
C	62.7
O	29.1
Si	4.5
N	2.0
S	0.9
Na	0.7
Zn	0.1
Ba	<0.1

8 Conclusions

LII excitation conditions encompass the laser fluence and wavelength while detection conditions specify the spectral and temporal collection parameters for the LII signal. Systems containing soot and PAHs illustrate the importance of judicious choice of excitation laser wavelength and detection timing interval. Both parameters allow minimizing excitation and detection of PAH fluorescence. Aerosols composed of either metals or oxides illustrate the need for proper choice of excitation laser fluence and detection wavelength.

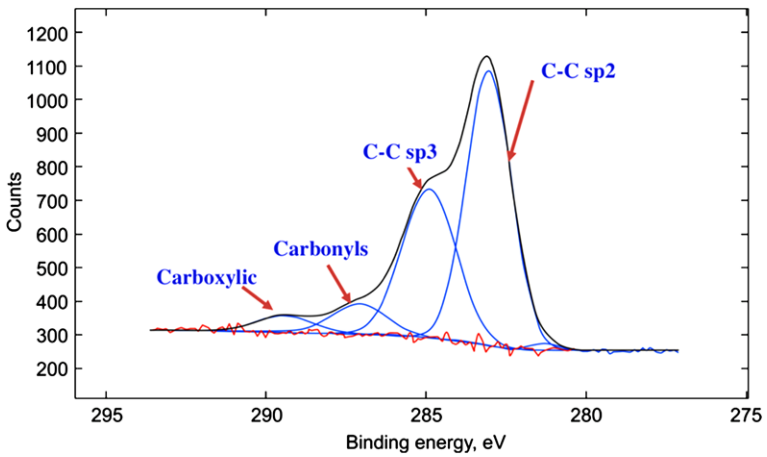

Fig. 5 XPS scan over the nominal C1s region. Deconvolution separates the sp^2 and sp^3 components. These may be interpreted as the elemental and organic components

This reflects the desire to produce and detect incandescence and not plasma emission arising from particle vaporization, given the lower melting and vaporization temperatures of metals and oxides relative to carbon.

The action of pulsed high intensity laser light can induce any number of possible changes in the absorbing aerosol. While particle heating resulting in incandescence is the ideal, aggregate fragmentation, coalescence or annealing are distinct possibilities. Notably, these changes necessarily occur on the time scale of LII, i.e. on the signal collection time scale.

Different diagnostics may be applied to detect the onset of and to quantify laser-induced aerosol changes. Spectrally resolved detection can reveal the onset and evolution of particle evaporation by super-elevated particle temperatures. Temporally resolved emission can identify structural changes if they affect the particle cooling rates (via either radiation or conduction). To probe the impact of physical and chemical changes upon the LII signal and identify their temporal onset requires an active diagnostic in the form of a pump–probe experiment. Finally, TEM of extracted material provides the best identification of the structural changes.

An aerosol can be 'mixed' in reference to chemistry, elemental bonding or both factors. In collecting the LII signal, one must be cognizant of the following factors: (a) the relative mass fractions of the different components, (b) the melting temperature and vaporization temperature differences of the components and (c) the reactivity of each material towards the other. Their specific challenge to LII is to identify the LII signal origin and its independence of either spatially or temporally changing aerosol chemistry.

As a relative diagnostic technique LII requires calibration. Several techniques can be applied including extinction, a two-color method, gravimetric sampling and comparison to a reference flame. Each of these methods has merits and limitations. As LII is applied to practical combustion systems operating at pressure, semi-empirical calibration may be required with models supplying a pressure correction factor to calibrations performed at atmospheric pressure.

Acknowledgements The author gratefully acknowledges support through the Keystone Innovation Starter Kit (KISK) grant through Penn State University, Contract No. C000032466 and the Penn States Institutes of Energy and the Environment (PSIEE). Engine samples and support for XPS analysis were supplied by Dr. Michael Hayes of the US EPA, National Risk Management Laboratory.

References

1. C. Schulz, B.F. Kock, M. Hofmann, H. Michelsen, S. Will, B. Bougie, R. Suntz, G. Smallwood, Appl. Phys. B: Lasers Opt. **83**, 333 (2006)
2. A. Eremin, E. Gurentsov, M. Hofmann, B. Kock, C. Schulz, Appl. Phys. B: Lasers Opt. **83**, 449 (2006)
3. Th. Lehre, B. Jungfleisch, R. Suntz, H. Bockhorn, Appl. Opt. **42**, 2021 (2003)
4. B. Axelsson, R. Collin, P.-E. Bengtsson, Appl. Opt. **39**, 683 (2000)
5. C. Allouis, A. D'Alessio, C. Noviello, F. Beretta, Combust. Sci. Technol. **153**, 51 (2000)
6. S. Schraml, S. Will, A. Leipertz, SAE Paper # 1999-01-0146 (1999)
7. A.V. Filippov, M.W. Markus, P. Roth, J. Aerosol Sci. **30**, 71 (1999)
8. S. Will, S. Schraml, K. Bader, A. Leipertz, Appl. Opt. **37**, 5647 (1998)
9. H.A. Michelsen, M.A. Linne, B.F. Kock, M. Hofmann, B. Tribalet, C. Schulz, Appl. Phys. B **93**, 645 (2008)
10. H.A. Michelsen, Appl. Phys. B **94**, 103 (2009)
11. F. Liu, K.J. Daun, D.R. Snelling, G.J. Smallwood, Appl. Phys. B: Lasers Opt. **83**, 355 (2006)
12. H. Bladh, P.-E. Bengtsson, Appl. Phys. B **78**, 241 (2004)
13. G.J. Smallwood, D.R. Snelling, F. Liu, O.L. Gulder, J. Heat Transfer **123**, 814 (2000)
14. K.J. Daun, G.J. Smallwood, F. Liu, J. Heat Transfer **130**, 121201-9 (2008)
15. A.V. Filippov, D.E. Rosner, Int. J. Heat Mass Transfer **43**, 127 (2000)
16. H.A. Michelsen, F. Liu, B.F. Kock, H. Bladh, A. Boiarciuc, M. Charwath, T. Dreier, R. Hadef, M. Hofmann, J. Reimann, S. Will, P.-E. Bengtsson, H. Bockhorn, F. Foucher, K.-P. Geigle, C. Mounaïm-Rousselle, C. Schulz, R. Stirn, B. Tribalet, R. Suntz, Appl. Phys. B **87**, 503 (2007)
17. R.L. Vander Wal, K.A. Jensen, M.Y. Choi, Combust. Flame **109**, 399 (1997)
18. R.L. Vander Wal, T.M. Ticich, G.M. Berger, P.D. Patel, Appl. Opt. **41**, 5678 (2002)
19. R.L. Vander Wal, M.Y. Choi, Carbon **37**, 231 (1999)
20. R.L. Vander Wal, T.M. Ticich, A.B. Stephens, Appl. Phys. B **67**, 115 (1998)
21. R.L. Vander Wal, in *26th Int. Combustion Symp.* (1996), pp. 2269–2275
22. http://www.cabot-corp.com/Silicas-And-Aluminas
23. R.L. Vander Wal, G.M. Berger, T.M. Ticich, J. Nanosci. Nanotechnol. **3**, 241 (2003)
24. R.L. Vander Wal, Carbon **40**, 2101 (2002)
25. R.L. Vander Wal, Combust. Flame **130**, 37 (2002)
26. R.L. Vander Wal, L.J. Hall, Combust. Flame **130**, 27 (2002)
27. R.L. Vander Wal, G.M. Berger, L.J. Hall, J. Phys. Chem. B **106**, 3564 (2002)
28. R.L. Vander Wal, Appl. Opt. **37**, 607 (1998)
29. R.L. Vander Wal, Appl. Opt. **35**, 6548 (1996)
30. H.A. Michelsen, P.O. Witze, D. Kayes, S. Hochgreb, Appl. Opt. **42**, 5577 (2003) and references therein
31. R.L. Vander Wal, Combust. Flame **110**, 281 (1997)
32. J.A. Steinfeld, *Molecules and Radiation: An Introduction to Modern Molecular Spectroscopy* (MIT Press, Cambridge, 1981)
33. R.L. Vander Wal, Combust. Flame **112**, 607 (1998)
34. R.L. Vander Wal, Combust. Sci. Technol. **118**, 343 (1996)
35. P.V. Kamat, J. Phys. Chem. B **110**, 21387 (2006)
36. R.L. Vander Wal, T.M. Ticich, J.R. West, Appl. Opt. **38**, 5867 (1999)
37. R.L. Vander Wal, A.J. Tomasek, K.W. Street, D.R. Hull, W.K. Thompson, Appl. Spectrosc. **58**, 230 (2004)
38. R.L. Vander Wal, A.J. Tomasek, Combust. Flame **134**, 1 (2003)
39. R.L. Vander Wal, K.-O. Lee, M.Y. Choi, Combust. Flame **102**, 200 (1995)
40. J.C. Reijenga (coordinator), *The Wondrous World of Carbon Nanotubes, A Review of Current Carbon Nanotube Technologies* (Eindhoven University, 2003). Available at http://students.chem.tue.nl/ifp03/Wondrous%20World%20of%20Carbon%20Nanotubes_Final.pdf

41. R.L. Vander Wal, L.J. Hall, Chem. Phys. Lett. **349**, 178 (2001)
42. R.L. Vander Wal, T.M. Ticich, J. Phys. Chem. B **105**, 10249 (2001)
43. R.L. Vander Wal, G.M. Berger, T.M. Ticich, Appl. Phys. A **77**, 885 (2003)
44. R.L. Vander Wal, T.M. Ticich, A.B. Stephens, Combust. Flame **116**, 291 (1998)
45. R.L. Vander Wal, T.M. Ticich, Appl. Opt. **38**, 1444 (1999)
46. S. De Iuliis, F. Migliorini, F. Cignoli, G. Zizak, Appl. Phys. B **83**, 397 (2006)
47. A. Boiarciuc, F. Foucher, C. Mounaim-Rousselle, Appl. Phys. B **83**, 413 (2006)
48. B.F. Kock, B. Tribalet, C. Schulz, P. Roth, Combust. Flame **147**, 79 (2006)
49. R.L. Vander Wal, Z. Zhou, M.Y. Choi, Combust. Flame **105**, 462 (1996)
50. T.C. Bond, Environ. Res. Lett. **2**, 045030-9 (2007)
51. R.L. Vander Wal, V.M. Bryg, M.D. Hayes, Environ. Sci. Technol. (submitted)